CHIN. PHYS. LETT. Vol. 37, No. 12 (2020) 120501

Active Thermal Wave Cloak

Liu-Jun Xu(须留钧)* and Ji-Ping Huang(黄吉平)*

Department of Physics, State Key Laboratory of Surface Physics, and Key Laboratory of Micro and Nano Photonic Structures (MOE), Fudan University, Shanghai 200438, China

(Received 2 October 2020; accepted 26 October 2020; published online 8 December 2020)

Active metamaterials have shown huge advantages to control electromagnetic and acoustic waves. However, how to use active metamaterials to control thermal waves has not been explored, though thermal waves are significant in various fields. To address the problem, here we report an active scheme for thermal wave cloaks. The thermal waves are based on conduction and convection, which are dominated by the Fourier and Darcy laws, respectively. By calculating the propagation of thermal waves in a free space, we can derive the global temperature and pressure distributions. We then apply these calculation results to actively control the boundary temperature and pressure, and active thermal wave cloaks can be obtained. Compared with existing passive schemes to control thermal waves, the present active scheme is more flexible for switching on/off and changing geometries. This work provides active and controllable components to thermal wave cloaks, which can be further used to design more active thermal wave metamaterials.

PACS: 05.70.−a, 44.10.+i, 81.05.Zx DOI: 10.1088/0256-307X/37/12/120501

Thermal invisibility is crucially important to fight against infrared detection, whose realization largely depends on the development of thermal metamaterials, especially thermal cloaks.[1] So far, the research scope of thermal metamaterials has been extended from conduction[2,3] to conduction-convection,[4−9] conduction-radiation,[10−13] and even conduction-convection-radiation.[14−16] Recently, the invisibility of thermal waves (i.e., the temperature has a wave form) has also attracted intensive research interest. The related explorations are mainly based on conduction,[17] conduction with thermal relaxation,[18] and conduction-convection.[19] For these different systems, the methods of scattering cancellation[17,18] and coordinate transformation[19] are successfully applied to achieve thermal wave invisibility.

However, these methods only apply to passive metamaterials, lacking the flexibility for switching on/off or changing geometries. Actually, active metamaterials have been widely applied to control physical fields such as electromagnetic waves,[20−22] acoustic waves,[23−25] fluid flows,[26,27] direct currents,[28−30] magnetic conduction,[31−33] and thermal conduction.[34−37] However, thermal wave cloaks still lack similar controllability. To solve the problem, here we study thermal waves based on conduction and convection, which are crucially important to achieve thermal phenomena such as anti-parity-time symmetry,[38,39] negative thermal transport,[40] and crystals.[41] Conduction and convection are dominated by the Fourier and Darcy laws, respectively. The discussed thermal waves can be treated as an ideal model of practical conditions. For example, there are temperature fluctuations in space, which can propagate via conduction and convection to generate thermal waves. We then consider two typical cases of thermal waves. The first one (case 1) is shown in Fig. 1(a), where the left and right boundaries are set with periodic boundary condition, leading to a zero imaginary part of thermal wave vector. The second one (case 2) is displayed in Fig. 1(b), where the left and right boundaries are set with time-harmonic temperature and open boundary condition, respectively. Therefore, the thermal wave has a nonzero imaginary part of thermal wave vector. We then calculate the propagation of thermal waves in a free space, and derive the global temperature and pressure distributions. By setting the boundary temperature and pressure as calculated, active thermal wave cloaks can be achieved. The controlled boundary is just the position surrounding the cloaked region. Let us start from the theory.

We consider a conduction-convection process in a porous medium composed of fluid and solid, whose dominant equation can be expressed as

$$\rho_{\mathrm{m}}C_{\mathrm{m}}\partial T/\partial t+\nabla\cdot(-\kappa_{\mathrm{m}}\nabla T+\rho_{\mathrm{f}}C_{\mathrm{f}}\boldsymbol{v}T)=0, \quad (1)$$

where $\rho_{\mathrm{m}}C_{\mathrm{m}}=\phi\rho_{\mathrm{f}}C_{\mathrm{f}}+(1-\phi)\rho_{\mathrm{s}}C_{\mathrm{s}}$, $\kappa_{\mathrm{m}}=\phi\kappa_{\mathrm{f}}+(1-\phi)\kappa_{\mathrm{s}}$, and ϕ are the effective product of density and heat capacity, effective thermal conductivity, and porosity of the porous medium,[42] respectively; ρ_{f} (ρ_{s}), C_{f} (C_{s}), and κ_{f} (κ_{s}) are the density, heat capacity, and thermal conductivity of the fluid (solid), respectively; T and t denote temperature and time, respectively; $\boldsymbol{v}$ is the convective velocity of the fluid. We suppose $\rho_{\mathrm{f}}C_{\mathrm{f}}=\rho_{\mathrm{s}}C_{\mathrm{s}}$ for brevity, so $\rho_{\mathrm{m}}C_{\mathrm{m}}=\rho_{\mathrm{f}}C_{\mathrm{f}}$. We then consider a thermal wave solution

$$T=Ae^{i(\beta x-\omega t)}+B, \quad (2)$$

where A, β, ω, and B are the temperature amplitude, wave vector, circular frequency, and reference temperature of the thermal wave, respectively; $i=\sqrt{-1}$ is the imaginary unit. Substituting Eq. (2) into Eq. (1)

Supported by the National Natural Science Foundation of China (Grant Nos. 11725521 and 12035004), and the Science and Technology Commission of Shanghai Municipality (Grant No. 20JC1414700).
*Corresponding authors. Email: 13307110076@fudan.edu.cn; jphuang@fudan.edu.cn

yields

$$-i\omega\rho_{\rm m}C_{\rm m}+\kappa_{\rm m}\beta^2+i\rho_{\rm f}C_{\rm f}v\beta=0. \tag{3}$$

We consider the first case with $\mathrm{Im}(\beta)=0$ and $\mathrm{Im}(\omega)\neq 0$ [see Fig. 1(a)], and Eq. (3) turns into

$$\omega=\frac{\rho_{\rm f}C_{\rm f}}{\rho_{\rm m}C_{\rm m}}v\beta-i\frac{\kappa\beta^2}{\rho_{\rm m}C_{\rm m}}. \tag{4}$$

Substituting Eq. (4) into Eq. (2) yields

$$T=Ae^{\mathrm{Im}(\omega)t}e^{i[\beta x-\mathrm{Re}(\omega)t]}+B, \tag{5}$$

which indicates that the thermal wave decays in time, but does not decay in space. Therefore, the thermal wave vector is preset, and the circular frequency is determined by the thermal wave vector.

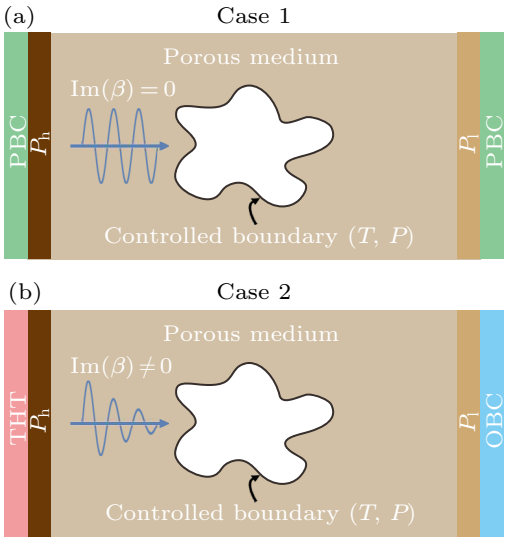

Fig. 1. Schematic diagrams of (a) case 1 and (b) case 2. PBC, periodic boundary condition; THT, time harmonic temperature; OBC, open boundary condition.

We then consider the second case with $\mathrm{Im}(\beta)\neq 0$ and $\mathrm{Im}(\omega)=0$ [see Fig. 1(b)], and Eq. (3) turns into

$$\beta=\frac{\sqrt{2}\gamma}{4}+i\frac{-8\rho_{\rm f}C_{\rm f}v\rho_{\rm m}C_{\rm m}\omega+2\sqrt{2}\rho_{\rm f}^2C_{\rm f}^2v^2\gamma+\sqrt{2}\kappa_{\rm m}^2\gamma^3}{16\rho_{\rm m}C_{\rm m}\omega\kappa_{\rm m}}, \tag{6}$$

where γ takes the form of

$$\gamma=\frac{\sqrt{-\rho_{\rm f}^2C_{\rm f}^2v^2+\sqrt{\rho_{\rm f}^4C_{\rm f}^4v^4+16\rho_{\rm m}^2C_{\rm m}^2\omega^2\kappa_{\rm m}^2}}}{\kappa_{\rm m}}. \tag{7}$$

Substituting Eq. (6) into Eq. (2) yields

$$T=Ae^{-\mathrm{Im}(\beta)x}e^{i[\mathrm{Re}(\beta)x-\omega t]}+B, \tag{8}$$

which indicates that the thermal wave decays in space, but does not decay in time. Therefore, the circular frequency is preset, and the thermal wave vector is determined by the circular frequency.

Convective velocities in the two cases are both determined by the steady Darcy law,[43–45]

$$\boldsymbol{v}=-\frac{\sigma}{\mu}\nabla P, \tag{9}$$

where σ is the permeability of the porous medium, μ is the dynamic viscosity of the fluid, and P denotes pressure. By setting a high pressure $P_{\rm h}$ on the left boundary and a low pressure $P_{\rm l}$ on the right boundary (see Fig. 1), the pressure profile can be expressed as

$$P=-\frac{P_{\rm h}-P_{\rm l}}{d}x+\frac{P_{\rm h}+P_{\rm l}}{2}, \tag{10}$$

where d is the distance between the left and right boundaries.

So far, we have derived all the information for designing active thermal wave cloaks, i.e., Eqs. (5), (8), and (10). Concretely speaking, Eqs. (5) and (10) can be applied for case 1 shown in Fig. 1(a), and Eqs. (8) and (10) can be applied for case 2 shown in Fig. 1(b).

To confirm the scheme, we further perform finite-element simulations based on COMSOL MULTIPHYSICS (http://www.comsol.com/). The results for cases 1 and 2 are presented in Figs. 2 and 3, respectively.

We firstly discuss case 1 (see Fig. 2). The boundary settings are the same as those in Fig. 1(a). The left and right boundaries are set with periodic boundary condition, which can be regarded as the temperature continuity of the left and right boundaries. The left and right boundaries are also set with high and low pressures, respectively. The upper and lower boundaries are set with no flux condition. The left three columns show the temperature profiles at 0, 100, and 200 s, respectively. The right column displays the pressure profiles, which do not change with time because we consider the steady Darcy law. The first and third rows exhibit the simulations with the central boundaries not actively controlled (i.e., only with no flux condition). The second and fourth rows exhibit the simulations with the central boundaries actively controlled by Eqs. (5) and (10). The initial temperature profiles are set at $T=40\cos(100\pi x)+323$ K (see the first column in Fig. 2). The origin locates at the center of each simulation. If the central boundaries are not actively controlled, the thermal waves and pressure profiles are strongly distorted [see Figs. 2(b)–2(d) and 2(j)–2(l)]. Fortunately, with the active control of central boundaries, the thermal waves can propagate without distortion, and the pressure profiles also become linear [see Figs. 2(f)–2(h) and 2(n)–2(p)]. As discussed, the thermal waves only decay in time, but do not decay in space.

We then discuss case 2 (see Fig. 3). Since the pressure settings are the same as those in Fig. 2, the pressure profiles are also the same as those in Fig. 2 (see the fourth column in Fig. 3). Differently, the periodic boundary condition is removed. Instead, the left boundary is set with time harmonic temperature, which can be expressed as $T=40\cos(-\pi t/10)+323$ K. The right boundary is set with open boundary condition, indicating no thermal wave reflection. The

initial temperature is set at 323 K (see the first column in Fig. 3). The results at 100 and 200 s are presented in the second and third columns of Fig. 3. Compared with the results without active control [see Figs. 3(b)–3(d) and 3(j)–3(l)], those with active control by Eqs. (8) and (10) are satisfying [see Figs. 3(f)–3(h) and 3(n)–3(p)]. Since the periodic boundary condition is replaced with time harmonic temperature and open boundary condition, the thermal waves only decay in space, but do not decay in time.

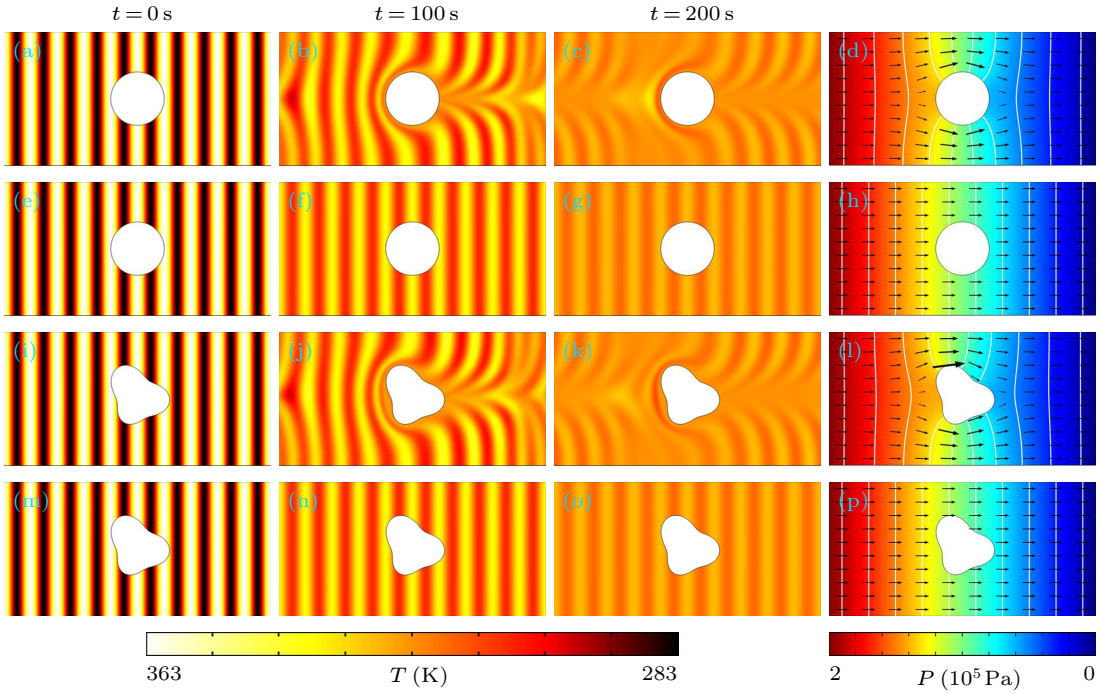

Fig. 2. Simulations of case 1 with (a)–(h) circular shape and (i)–(p) arbitrary shape. The simulation size is $20 \times 10\,\mathrm{cm}^2$. The circular shape in the first two rows has a radius of 2 cm. The arbitrary shape in the last two rows has a radius of $2 + 0.2\sin\theta - 0.2\sin(2\theta) + 0.4\cos(3\theta)$ cm. The temperature of the controlled boundary is $T = 40e^{-\pi^2 t/10^3}\cos(100\pi x - \pi t/10) + 323\,\mathrm{K}$, and the pressure of the controlled boundary is $P = -10^6 x + 10^5$ Pa. Parameters: $\rho_\mathrm{m}C_\mathrm{m} = \rho_f C_f = 10^6\,\mathrm{J{\cdot}m^{-3}{\cdot}K^{-1}}$, $\kappa_\mathrm{m} = \kappa_\mathrm{f} = 0.1\,\mathrm{W{\cdot}m^{-1}{\cdot}K^{-1}}$, $\sigma = 10^{-12}\,\mathrm{m}^2$, $\mu = 10^{-3}\,\mathrm{Pa{\cdot}s}$, $P_\mathrm{h} = 2 \times 10^5$ Pa, and $P_\mathrm{l} = 0$ Pa. Lines and arrows in the last column denote isobars and velocities, respectively.

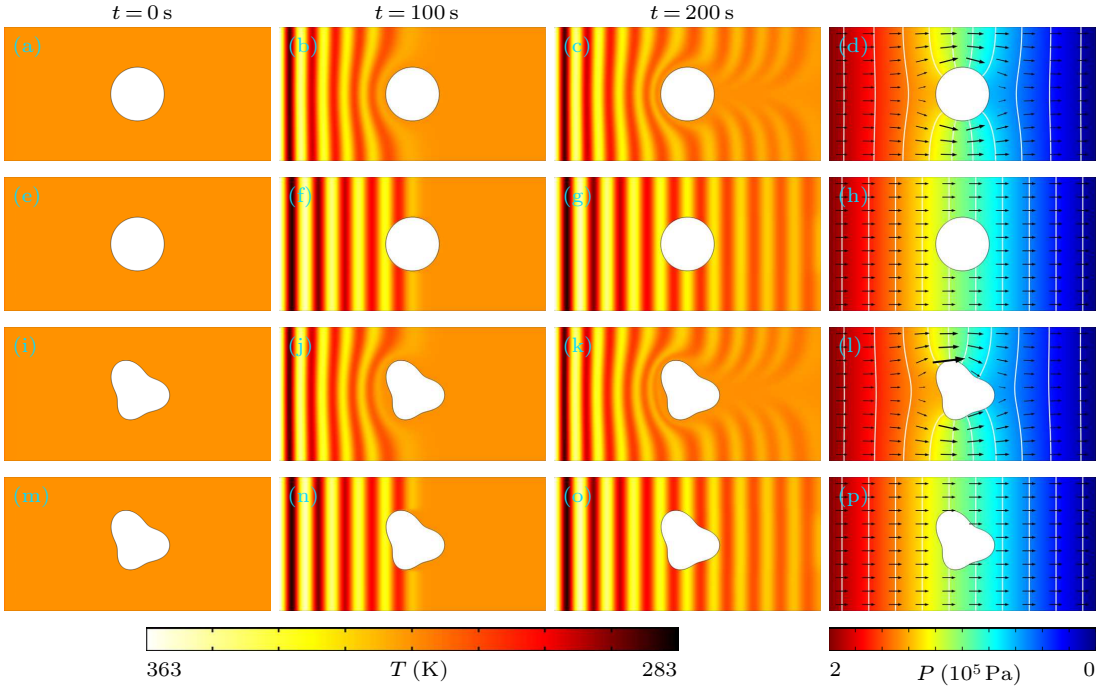

Fig. 3. Simulations of case 2 with (a)–(h) circular shape and (i)–(p) arbitrary shape. The sizes and parameters are the same those in Fig. 2. The temperature of the controlled boundary is $T = S(t)40e^{-9.82(x+0.1)}\cos[313.54(x + 0.1) - \pi t/10] + 323\,\mathrm{K}$, and the pressure of the controlled boundary is $P = -10^6 x + 10^5$ Pa. $S(t)$ is a step function with $S(t \le 100) = 0$ and $S(t > 100) = 1$.

The results shown in Figs. 2 and 3 are satisfying because we apply ideal settings such as a continuous temperature control and a continuous pressure control on the central boundary. However, it might be challenging to continuously control the temperature and pressure in experiments. To solve this experimental difficulty, we further discrete the temperature and pressure, and the results are shown in Fig. 4. We apply 36 small circles with diameter 1 mm around the central boundary to control the temperature and pressure. The first and last two rows show the results of cases 1 and 2, respectively. The left three columns exhibit the temperature profiles at 0, 100, 200 s, respectively. The last column presents the pressure profiles. Clearly, the cloaking effect is also achieved, though it is not as perfect as that based on ideal settings. Moreover, to reduce experimental difficulty, one can increase the periodicity of the thermal wave, and control the temperature by alternately using ceramic heater and semiconductor cooler.

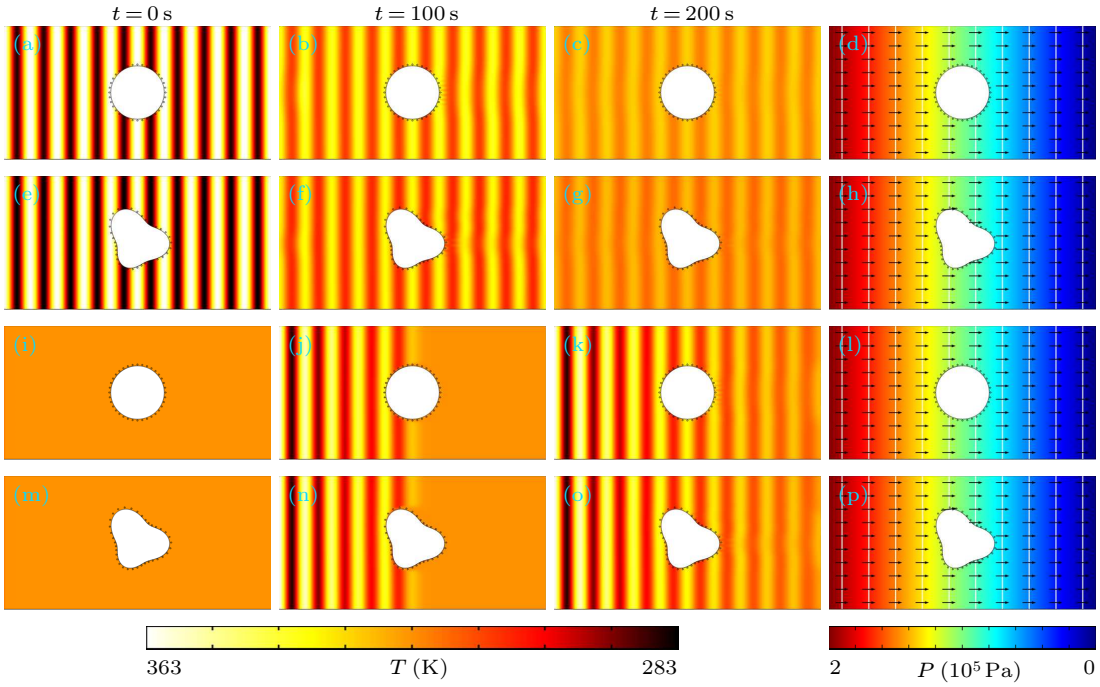

Fig. 4. Discrete boundary control of (a)–(h) case 1 and (i)–(p) case 2. The settings are the same as those in Figs. 2 and 3 except for the central boundary. There are 36 circles with diameter 1 mm arranged every 10 deg.

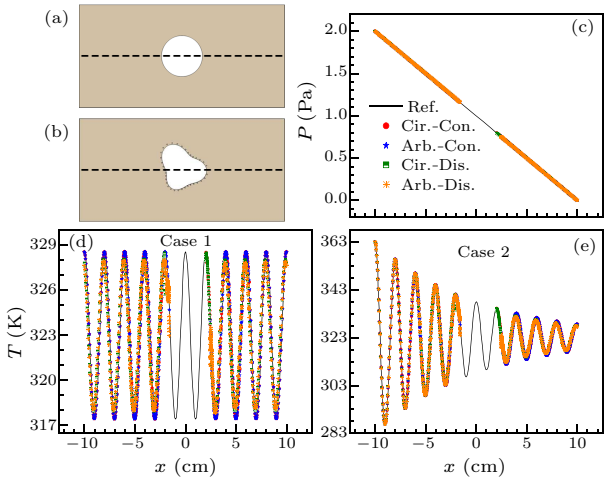

Fig. 5. Quantitative comparison. (a) Circular shape with continuous control (abbreviated as Cir.-Con.). (b) Arbitrary shape with discrete control (abbreviated as Arb.-Dis.). Similarly, Arb.-Con., arbitrary shape with continuous control; Cir.-Dis., circular shape with discrete control. (c) Pressure distribution of case 1 (which is the same as case 2). Temperature distribution at 200 s of (d) case 1 and (e) case 2.

To compare the cloaking effect quantitatively, we further plot the data of the pressure and temperature along the x axis [i.e., on the dashed lines in Figs. 5(a) and 5(b)]. Since the pressure profiles of cases 1 and 2 are the same, we only plot the pressure profiles of case 1 for brevity [see Fig. 5(c)]. The solid line is a reference with no obstacle in the center. Cir.-Con. means circular shape with continuous control [see Fig. 5(a)], and Arb.-Dis. means arbitrary shape with discrete control [see Fig. 5(b)]. Similarly, Arb.-Con. and Cir.-Dis. means arbitrary shape with continuous control and circular shape with discrete control, respectively. Obviously, with the active control, whether continuously or discretely, the pressure profiles are the same as the reference (i.e., the five lines overlap). The temperature profiles with continuous control (at 200 s) are also the same as the reference, and those with discrete control have only a smaller temperature amplitude than the reference [see Figs. 5(d) and 5(e)]. Therefore, the active scheme is experimentally feasible.

We have discussed the thermal waves based on conduction and convection. Actually, many other systems can also support the propagation of thermal waves. Especially, thermal waves based on modifying the Fourier law with thermal relaxation have been long investigated.[46–50] Therefore, how to use an active scheme to control these thermal waves remains to be explored. Moreover, the active scheme

requires to know the temperature and pressure distributions in advance. For practical applications, machine learning[51] might be applied to obtain global information by only detecting local information, and provides guidance for the active control.

In summary, we have proposed an active scheme for thermal wave cloaks. By actively controlling the boundary temperature and pressure, we can construct a cloaked region, outside which thermal waves can propagate without distortion. The feasibility of the scheme is confirmed by finite-element simulations with both continuous and discrete boundary control. This scheme has superiorities such as switching on/off flexibly and designing irregular geometries. Our work provides active and controllable components to thermal wave metamaterials, which are desirable in many practical applications like thermal wave imaging[52–56] and thermal illusion.[57–60]

References

[1] Huang J P 2020 *Theoretical Thermotics: Transformation Thermotics and Extended Theories for Thermal Metamaterials* (Berlin: Springer)
[2] Fan C Z, Gao Y and Huang J P 2008 *Appl. Phys. Lett.* **92** 251907
[3] Chen T Y, Weng C N and Chen J S 2008 *Appl. Phys. Lett.* **93** 114103
[4] Guenneau S, Petiteau D, Zerrad M, Amra C and Puvirajesinghe T 2015 *AIP Adv.* **5** 053404
[5] Dai G L, Shang J and Huang J P 2018 *Phys. Rev. E* **97** 022129
[6] Li Y, Zhu K J, Peng Y G, Li W, Yang T Z, Xu H X, Chen H, Zhu X F, Fan S H and Qiu C W 2019 *Nat. Mater.* **18** 48
[7] Yang F B, Xu L J and Huang J P 2019 *ES Energy & Environ.* **6** 45
[8] Yeung W S, Mai V P and Yang R J 2020 *Phys. Rev. Appl.* **13** 064030
[9] Xu L J and Huang J P 2020 *Sci. Chin. Phys. Mech. & Astron.* **63** 228711
[10] Li Y, Bai X, Yang T Z, Luo H L and Qiu C W 2018 *Nat. Commun.* **9** 273
[11] Xu L J and Huang J P 2019 *Phys. Rev. Appl.* **12** 044048
[12] Peng Y G, Li Y, Cao P C, Zhu X F and Qiu C W 2020 *Adv. Funct. Mater.* **30** 2002061
[13] Xu L J, Dai G L and Huang J P 2020 *Phys. Rev. Appl.* **13** 024063
[14] Xu L J, Yang S, Dai G L and Huang J P 2020 *ES Energy & Environ.* **7** 65
[15] Wang J, Yang F B, Xu L J and Huang J P 2020 *Phys. Rev. Appl.* **14** 014008
[16] Yang S, Xu L J, Dai G L and Huang J P 2020 *J. Appl. Phys.* **128** 095102
[17] Farhat M, Chen P Y, Bagci H, Amra C, Guenneau S and Alù A 2015 *Sci. Rep.* **5** 9876
[18] Farhat M, Guenneau S, Chen P Y, Alù A and Salama K N 2019 *Phys. Rev. Appl.* **11** 044089
[19] Xu L J and Huang J P 2020 *Int. J. Heat Mass Transfer* **159** 120133
[20] Vasquez F G, Milton G W and Onofrei D 2009 *Phys. Rev. Lett.* **103** 073901
[21] Selvanayagam M and Eleftheriades G V 2013 *Phys. Rev. X* **3** 041011
[22] Kord A, Sounas D L and Alù A 2018 *Phys. Rev. Appl.* **10** 054040
[23] Vasquez F G, Milton G W and Onofrei D 2011 *Wave Motion* **48** 515
[24] Ning L, Wang Y Z and Wang Y S 2020 *Int. J. Solids Struct.* **202** 126
[25] Kerferd B, Eggler D, Karimi M and Kessissoglou N 2020 *J. Sound Vib.* **479** 115400
[26] Urzhumov Y A and Smith D R 2012 *Phys. Rev. E* **86** 056313
[27] Culver D and Urzhumov Y 2017 *Phys. Rev. E* **96** 063107
[28] Ma Q, Mei Z L, Zhu S K, Jin T Y and Cui T J 2013 *Phys. Rev. Lett.* **111** 173901
[29] Lan C W, Bi K, Gao Z H, Li B and Zhou J 2016 *Appl. Phys. Lett.* **109** 201903
[30] Chen T H, Zheng B, Yang Y H, Shen L, Wang Z J, Gao F, Li E P, Luo Y, Cui T J and Chen H S 2019 *Light: Sci. & Appl.* **8** 30
[31] Mach-Batlle R, Parra A, Laut S, Del-Valle N, Navau C and Sanchez A 2018 *Phys. Rev. Appl.* **9** 034007
[32] Jiang W, Ma Y G and He S L 2018 *Phys. Rev. Appl.* **9** 054041
[33] Dai X and Jiang J C 2020 *AIP Adv.* **10** 025211
[34] Nguyen D M, Xu H Y, Zhang Y M and Zhang B L 2015 *Appl. Phys. Lett.* **107** 121901
[35] Guo J and Qu Z G 2018 *Int. J. Heat Mass Transfer* **127** 1212
[36] Xu L J, Yang S and Huang J P 2019 *Phys. Rev. E* **100** 062108
[37] Xu L J, Yang S and Huang J P 2020 *Europhys. Lett.* **131** 24002
[38] Li Y, Peng Y G, Han L, Miri M A, Li W, Xiao M, Zhu X F, Zhao J L, Alù A, Fan S H and Qiu C W 2019 *Science* **364** 170
[39] Cao P C, Li Y, Peng Y G, Qiu C W and Zhu X F 2020 *ES Energy & Environ.* **7** 48
[40] Xu L J and Huang J P 2020 *Chin. Phys. Lett.* **37** 080502
[41] Xu L J and Huang J P 2020 *Appl. Phys. Lett.* **117** 011905
[42] Bear J and Corapcioglu M Y 1984 *Fundamentals of Transport Phenomena in Porous Media* (Berlin: Springer)
[43] Urzhumov Y A and Smith D R 2011 *Phys. Rev. Lett.* **107** 074501
[44] Park J, Youn J R and Song Y S 2019 *Phys. Rev. Lett.* **123** 074502
[45] Park J, Youn J R and Song Y S 2019 *Phys. Rev. Appl.* **12** 061002
[46] Joseph D D and Preziosi L 1989 *Rev. Mod. Phys.* **61** 41
[47] Nie B D and Cao B Y 2019 *Int. J. Heat Mass Transfer* **135** 974
[48] Gandolfi M, Benetti G, Glorieux C, Giannetti C and Banfi F 2019 *Int. J. Heat Mass Transfer* **143** 118553
[49] Simoncelli M, Marzari N and Cepellotti A 2020 *Phys. Rev. X* **10** 011019
[50] Domenico M D, Jou D and Sellitto A 2020 *Int. J. Heat Mass Transfer* **156** 119888
[51] Hu R, Iwamoto S, Feng L, Ju S H, Hu S Q, Ohnishi M, Nagai N, Hirakawa K and Shiomi J 2020 *Phys. Rev. X* **10** 021050
[52] Orth T, Netzelmann U and Pelzl J 1988 *Appl. Phys. Lett.* **53** 1979
[53] Busse G, Wu D and Karpen W 1992 *J. Appl. Phys.* **71** 3962
[54] Mulaveesala R and Tuli S 2006 *Appl. Phys. Lett.* **89** 191913
[55] Mulaveesala R and Tuli S 2008 *AIP Conf. Proc.* **1004** 15
[56] Tuli S and Chatterjee K 2012 *AIP Conf. Proc.* **1430** 523
[57] Sha W, Zhao Y T, Gao L, Xiao M and Hu R 2020 *J. Appl. Phys.* **128** 045106
[58] Hu R, Huang S Y, Wang M, Luo X B, Shiomi J and Qiu C W 2019 *Adv. Mater.* **31** 1807849
[59] Hu R, Zhou S L, Li Y, Lei D Y, Luo X B and Qiu C W 2018 *Adv. Mater.* **30** 1707237
[60] Hu R, Huang S Y, Wang M, Zhou L L, Peng X Y and Luo X B 2018 *Phys. Rev. Appl.* **10** 054032